Fundamental Research 5 (2025) 183–191

Contents lists available at ScienceDirect

Fundamental Research

journal homepage: http://www.keaipublishing.com/en/journals/fundamental-research/

Article

Mannan-decorated STING-activating vaccine carrier for spatial coordinative stimulating antigen-specific immune responses

Liping Liu[a,b], Jiayu Zhao[a,b], Zichao Huang[a,b], Yudi Xu[a], Hongyu Chen[a,b], Ruirui Qiao[d], Wantong Song[a,b,c,*], Zhaohui Tang[a,b,c,*], Thomas P. Davis[d], Xuesi Chen[a,b,c]

[a] Key Laboratory of Polymer Ecomaterials, Changchun Institute of Applied Chemistry, Chinese Academy of Sciences, Changchun 130022, China
[b] University of Science and Technology of China, Hefei 230026, China
[c] Jilin Biomedical Polymers Engineering Laboratory, Changchun 130022, China
[d] Australian Institute of Bioengineering and Nanotechnology, The University of Queensland, Brisbane, Queensland 4072, Australia

ARTICLE INFO

Article history:
Received 9 December 2022
Received in revised form 13 March 2023
Accepted 26 March 2023
Available online 11 May 2023

Keywords:
Cancer immunotherapy
Cancer vaccine
Nanotechnology
Drug delivery
Biopolymer

ABSTRACT

In recent years, the use of nanotechnologies to improve immunotherapy efficiency has attracted increasing interest in preventive and therapeutic cancer vaccine design. However, current nanocarriers are restricted by difficulties in the systematic spatial coordinative transport of antigens, which greatly hampers the immune response efficacy of nanovaccines. Herein, we designed a mannan-decorated stimulator of the interferon genes (STING)-activating vaccine carrier for spatial coordinative stimulation of antigen-specific immune responses and elicitation of robust antitumor immunity. Mannan-decoration as the shell could significantly enhance the lymph node draining ability of the nanovaccines, especially in $CD8^+$ dendritic cells (DCs). Azole molecule end-capped polylactic acid-polyethylenimine (PLA-PEI-4BImi) with innate stimulating activity was applied as the inner core for coordinating antigen-presenting cell activation and antigen cross-presentation. In the in vivo therapy study, single usage of this nanovaccine could achieve a 93% tumor suppression rate in the B16-OVA tumor model, which is superior to the commercialized aluminum adjuvant. This study demonstrates that a rational design of vaccine carriers for solving spatial transmission issues could greatly improve cancer vaccine efficiencies.

1. Introduction

Great success has been made in the field of tumor immunology in recent years [1], especially with the rapid progression in immune checkpoint inhibitors and adoptive cell transfer (ACT) therapy [2–4]. Owing to their high specificity, long-lasting efficacy, and safety, therapeutic cancer vaccines, another promising immunotherapy method, are quickly becoming a focus in cancer immunotherapy research [5–7]. By activating the immune response of patients, cancer vaccines can enhance the anticancer ability, achieve the purpose of tumor control or radiation, and prevent tumor recurrence [8–10]. However, owing to inefficient vaccine delivery, current vaccines often lead to a low immune response rate, which greatly hinders the translation of vaccines into clinic [11]. Therefore, enhancing the efficiency of each process in vaccine delivery has tremendous significance for eliciting a robust antitumor immune response to cancer vaccines.

Generally, exerting the efficient immune effect of cancer vaccines requires complicated multistep spatial transport of antigens, which mainly includes draining from the administration site to the lymph nodes, deep penetration to the paracortex of lymph nodes, uptake by and maturation of antigen-presenting cells (APCs), and antigen cross-presentation to $CD8^+$ T cells [9]. The effective accumulation of antigens in lymph nodes, the fundamental organs of the adaptive immune system, is the precondition for a cancer vaccine to exert a robust antitumor immune response [12,13]. It has been well characterized that surface shielding can enhance nanoparticle drainage through afferent lymphatic vessels [14]. In addition, the combination of passive draining and active cell-mediated transport can greatly increase the accumulation of nanovaccines in lymph nodes. For example, mannan-decorated nanovaccines, owing to their specific binding with mannose receptors on APCs, could effectively migrate to draining lymph nodes and be deeply delivered to $CD8^+$ DCs to elicit robust antitumor cytotoxic T lymphocyte (CTL) immune responses [15]. The spatial coordination of innate stimulation of APCs and antigen cross-presentation has been recognized as an essential process of antigen-specific immune responses in cancer vaccines [16]. Release of antigen into the cytoplasm is essential for cross-presenting antigens to $CD8^+$ T cells via the major histocompatibility complex class I (MHC I). However, the pattern recognition receptors (PRRs) of currently

* Corresponding authors.
E-mail addresses: wtsong@ciac.ac.cn (W. Song), ztang@ciac.ac.cn (Z. Tang).

https://doi.org/10.1016/j.fmre.2023.03.018

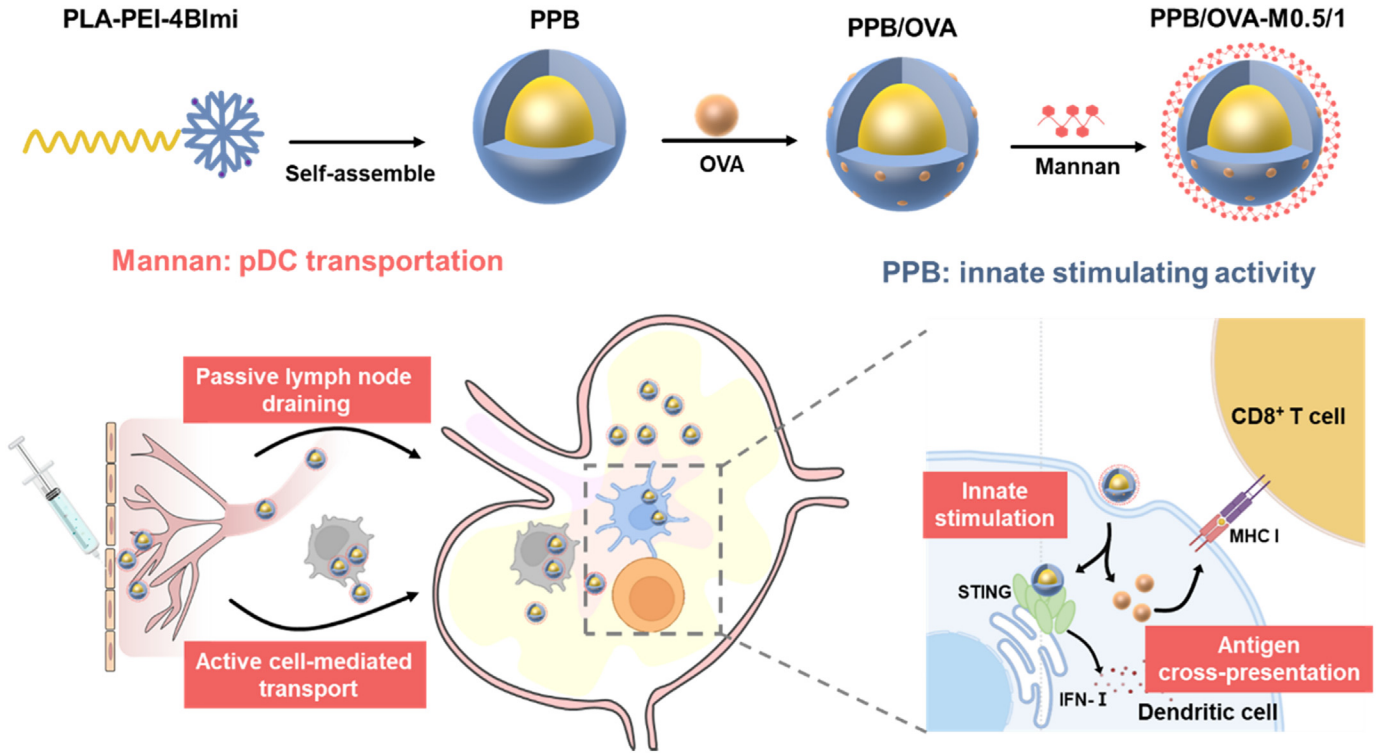

Scheme 1. Schematic illustration of the mannan-decorated STING-activating vaccine carrier design and the mechanism in systematically spatially coordinated stimulation of antigen-specific immune responses. PPB/OVA-M0.5/1 consists of self-assembled PLA-PEI-4BImi as a core, adsorption of OVA using electrostatic interaction and modification of mannan on the shell. Mannan-decoration could greatly enhance the accumulation of nanovaccines in lymph node via passive draining and active cell-mediated transport. PPB, as the innate stimulation core, could perform antigen cross-presentation while activating the antigen-presenting cells through the STING pathway.

used adjuvants are mainly located in the endosome [17]. The agonist of cytoplasm PRRs, such as cyclic guanosine monophosphate-adenosine monophosphate (cGAMP) against the cytoplasm STING pathway, provides a possible solution for resolving the obstacle of complicated positions of APC activation and antigen cross-presentation. However, there has been no report on designing such a vaccine system for systematic spatial coordination of the process from lymph node accumulation to antigen cross-presentation to $CD8^+$ T cells [18–20].

Herein, a mannan-decorated STING-activating vaccine carrier was designed for spatial coordinative stimulation of antigen-specific immune responses (Scheme 1). Mannan, as a yeast-derived polysaccharide, can be detected and bound to immature DCs, mainly through combination with the mannose receptor and DC-specific intercellular adhesion molecule 3-grabbing non-integrin (DC-SIGN), thus improving the ability of antigen-presenting cells (APCs) recognition and lymph node accumulation [15,21,22]. The azole molecule end-capped polyethyleneimine (PEI-4BImi) was proven in our previous study to have innate stimulating activity via activation of the STING pathway [23]. In this work, PEI-4BImi was further grafted with hydrophobic polylactide (PLA) to further increase its stability while maintaining the stimulatory activity of the STING pathway. In the preparation process, PLA-PEI-4BImi (we name it PPB for short) was self-assembled as the inner core, and antigen proteins (OVA) were absorbed through electrostatic interactions onto the nanoformulations. Finally, oxidized mannan was decorated on the surface by forming Schiff's base bonds between the aldehyde and amine groups. We showed that the mannan-decorated STING-activating vaccine carrier (PPB/OVA-M1) could greatly increase the accumulation capacity in lymph nodes and eliminate the obstacle in intracellular coordination of APC activation and antigen cross-presentation to $CD8^+$ cytotoxic T cells, thus resulting in better therapeutic effects in the B16-OVA tumor model. These results indicate the necessity of spatially controllable vaccines in therapy and provide inspiration and reference for the study of tumor vaccine carriers.

2. Materials and methods/experiment

2.1. Materials

Lactide monomer was generously donated by Changchun SinoBiomaterials Co., Ltd. Branched polyethyleneimine (M.W. 10kDa, PEI10K) was purchased from Alfa Asear. Benzoimidazole-4-carboxylic acid (4BImi) was purchased from Shanghai Aladdin Biochemical Technology Co., Ltd. Mannan (from yeast) was purchased from Sigma Aldrich Co., Ltd. Ovalbumin (OVA, chicken egg white) was purchased from Sigma–Aldrich Co., Ltd. Brefeldin A (BFA) was purchased from MedChemExpress. 2′,3′-cGAMP sodium was purchased from MedChemExpress. IFN-β mouse uncoated ELISA kit was purchased from R&D Systems. Aluminum adjuvant was purchased from Thermal Fisher Co. Ltd. The IFN-γ ELISPOT set was purchased from BD Biosciences. Antibodies for flow cytometry and western blot were purchased from BioLegend Co., Ltd. and Cell Signaling Technology, Inc. (Table S1).

2.2. Methods

2.2.1. Cell lines

DC2.4 cells (mouse dendritic cell line) were cultured in RPMI-1640 (containing 10% fetal bovine serum (FBS), 100 U/mL penicillin, and 100 μg/mL streptomycin) at 37 °C in an atmosphere of 5% CO_2. B16-OVA cells (murine B16 melanomas) were cultured in DMEM (containing 10% FBS, 100 U/mL penicillin, and 100 μg/mL streptomycin) at 37 °C in an atmosphere of 5% CO_2.

2.2.2. Animal declaration

All animal studies were carried out according to the guidelines approved by the Animal Welfare and Ethics Committee of Changchun Institute of Applied Chemistry, Chinese Academy of Sciences (2022–0026). Female C57BL/6 mice (6–8 weeks) were purchased from Beijing Vital River Laboratory Animal Technology Co., Ltd. (Beijing, China). Mice were sacrificed and recorded as death when the tumor volume reached 2,000 mm^3.

2.2.3. Preparation and characterization of nanovaccines

For the preparation of PPB, PLA was first synthesized by ring-opening polymerization of lactide with stannous octanoate as a catalyst and then grafted onto PEI. Briefly, PLA (1 mmol, 1 eq.) was first dissolved in anhydrous DMSO, to which CDI (1.2 mmol, 1.2 eq.) was added. PEI (1 mmol, 1 eq.) dissolved in anhydrous DMSO was added after 12 h of stirring at room temperature (RT).

PLA-PEI-4BImi was synthesized through an amide condensation reaction using EDC·HCl and NHS as condensation agents. 4BImi (1 mmol, 20 eq.), PLA-PEI (0.025 mmol, 1 eq.), EDC·HCl (1.5 mmol, 30 eq.), and NHS (2 mmol, 40 eq.) were dissolved in DMSO. After 72 h, the acquired products were dialyzed against water with a pH gradient from pH 3 to pH 7. The final product was obtained after lyophilization.

PLA-PEI (300 MHz, D_2O, ppm): 4.06 (m, 60H), 3.54 (m, 930H, -($CH_2CH_2NH)_n$-), 1.26 (m, 178H).

PLA-PEI-4BImi (300 MHz, D_2O + DCl, ppm): 8.94 (m, 21H), 7.39 (m, 60H), 4.06 (m, 64H), 3.54 (m, 930H, -($CH_2CH_2NH)_n$-), 1.26 (m, 179H).

The oxidized mannan was synthesized by dissolving 329 mg of mannan in 20 ml of sterile water, which was stirred in ice bath conditions, and 197.4 mg of sodium periodate was slowly added to the cooled mannan solution. After reacting overnight in the dark, the mannan was dialyzed and lyophilized in sterile water to obtain oxidized mannans at 30% oxidation.

For the preparation of nanovaccines PPB/OVA-M0.5 and PPB/OVA-M1, the OVA (1.0 mg/mL) solution was added dropwise to the PLA-PEI-4BImi solution (3.0 mg/mL) under vortexing at a volume ratio of 1:1; then, the oxidized mannan solution (1.0 mg/mL) was added at a weight ratio of 1:0.5 and 1:1. Zetasizer Nano ZS (Malvern Panalytical Co. Ltd.) was used to measure the diameters and zeta potentials.

2.2.4. ELISA detection of IFN-β release

DC2.4 cells (0.8×10^4 per well) were seeded in a 96-well plate, and after overnight incubation, different vaccine formulations at a final concentration of 20 μg OVA/mL were added. The supernatant was collected after an additional 24 h of incubation. Cytokine levels were detected in the supernatant of cultured DC2.4 cells using a mouse IFN-β ELISA kit with the manufacturer's protocol as the standard.

2.2.5. FACS analysis of phosphorylation expression of STING pathway-related proteins

To analyze the phosphorylation levels of STING pathway-related proteins in BMDCs, cells were incubated with a final concentration of 20 μg OVA/mL for 4 h. Subsequently, the cells were harvested and processed as follows: washed once with PBS, mixed with 4% PFA for 15 min at RT, washed again, permeabilized with 90% methanol for 10 min on ice, washed twice, and stained with antibody cocktail for 1 h. Finally, the cells were resuspended in PBS for FACS analysis.

2.2.6. CLSM imaging of STING protein clustering

DC2.4 cells (3×10^5 per well) were seeded in different confocal Petri dishes with 1.5 mL of RPMI 1640 medium containing different vaccine formulations at a final concentration of 20 μg OVA/mL and incubated for 4 h. Then, all cells were mixed with 4% PFA for 15 min, permeabilized with 0.1% Triton X-100 for 15 min, and stained with rabbit anti-human STING antibody (1:50 diluent in PBS) for 45 min, and a secondary FITC-conjugated donkey anti-rabbit antibody (1:50 diluent in PBS) were coincubated for 20 min and then incubated with DAPI (10 μg/mL in PBS) for 10 min. Finally, DC2.4 cells were incubated in PBS for CLSM (Carl Zeiss LSM 710, Germany) imaging.

2.2.7. Cellular uptake

DC2.4 cells were seeded at 1.5×10^5 cells in 24-well plates. Various vaccine formulations were prepared using OVA-Cy5 in the same procedure as described above. The different vaccines were added to each well for different treatment groups. The final OVA equivalent concentration was 20 μg/mL. All cells were collected and processed for flow cytometry analysis after 4 h of incubation.

2.2.8. BMDCs activation and antigen cross-presentation

In the in vitro DC activation assay, BMDCs were seeded at 4×10^5 cells per well in 24-well plates. The different vaccine formulations in each well were 20 μg OVA/mL for 4 h incubation. All cells were collected and processed and then labeled with an antibody cocktail (anti-FITC–CD11c, APC–Cy7-MHCII, APC–CD80 antibodies) for flow cytometry analysis.

In the in vitro antigen cross-presentation assay, BMDCs were seeded at 4×10^5 cells per well in 24-well plates. Different vaccine formulations were added to each well of different treatment groups. The final concentration of OVA was 20 μg/mL. After 24 h of incubation, all groups were gently collected and processed and then labeled with an antibody cocktail (anti-APC–CD11c, PE-H2Kb antibodies) for flow cytometry analysis.

2.2.9. Flow cytometry analysis of lymph node accumulation

The accumulation of various vaccine formulations in the LNs was carried out by fluorescence imaging and flow cytometry. Vaccine formulations were prepared using OVA-Cy5 instead of OVA in the same procedure as described above. Six- to eight-week-old female C57BL/6 mice were randomly grouped and injected subcutaneously (100 μg OVA in total) on the left and right sides of the tail base. Twenty-four hours later, the different treated mice were executed, and the lymph nodes on both inguinal sides were excised, one for fluorescence analysis and the other for flow cytometry analysis (BD FACS Celesta). For flow cytometry processing, all inguinal lymph nodes were completely ground. The single-cell suspensions obtained were labeled with an antibody cocktail (anti-PE-CD11c, APC–Cy7-MHC, Alexa Fluor 700-CD8a, and FITC-Siglec).

2.2.10. Western blot analysis

DC2.4 cells were seeded at 1×10^6 cells in 6-well plates. The different formulations were added to each well for different treatment groups. The final OVA equivalent concentration was 20 μg/mL. For the inhibitor assay, cells were pretreated with BFA (10 μM) for 1 h before different formulations addition.

Briefly, cells were lysed in SDS loading buffer (containing protease and phosphatase inhibitor cocktail) and denatured by heating. The supernatant was loaded onto a 12% SDS-PAGE gel and run for 80 min at 80 V. After transfer, the membranes were incubated for 45 min at room temperature in blocking solution and incubated with primary antibody at 4 °C overnight. Goat anti-rabbit or goat anti-mouse IgG enzyme-linked secondary antibodies (1:1000) were incubated for 60 min. Western blot images were obtained by an Amersham Imager 600 (AI600, General Electric Co., Ltd., USA) with 300 μL of ECL chemiluminescent reagent added on top of the membrane.

2.2.11. FACS analysis of DC activation in LNs

For DC activation in LNs, C57BL/6 mice were injected subcutaneously with different OVA vaccine formulations at the base of the tail. After 48 h, inguinal LNs were removed, and a single-cell suspension was obtained after grinding and filtering. The collected cells were labeled with an antibody cocktail (anti-CD11c, MHCII, CD80, CD86, and SIINFEKL-H2Kb antibodies) for FACS analysis.

2.2.12. Tumor growth inhibition

A subcutaneous B16-OVA tumor model was developed by injecting 2.5×10^5 cells into the right flank of 6- to 8-week-old female C57BL/6 mice. Tumor-bearing mice were randomized into groups and inoculated subcutaneously at the tail base with PBS, Alum/OVA, PPB/OVA, and PPB/OVA-M1 on Days 5, 10, and 15 after tumor cell inoculation. Alum/OVA formulations were prepared by mixing a one-time dilution of Inject Alum adjuvant with an equal volume of OVA solution. The single injection dose was 50 μg OVA per mouse. Tumor volume and body weight were recorded every two days. The tumor volume was obtained from Vernier caliper measurements and calculated as follows: tumor volume (V) = $a \times b^2/2$, where a represents the long axis and b represents the short axis of the tumor.

2.2.13. ELISPOT assay

The antigen-specific response of T cells secreting IFN-γ was determined using the ELISPOT assay. On 96-well ELISPOT plates, 100 μl of capture anti-IFN-γ antibody diluent was incubated at 4 ˚C overnight, followed by blocking with 10% FBS in PBS for 2 h. OVA protein containing RPMI 1640 was then added. Fresh mouse splenic cells from different treatment groups were inoculated in each well at 3×10^5 cells per well. Cells were then incubated at 37 ˚C for 72 h. The anti-IFN-γ detection antibody diluent was incubated for 2 h at RT. Enzyme coupling (streptavidin-HRP) was incubated for 1 h at RT, and AEC solution was added to each well for 30 min. Monitoring the development of spots was performed by terminating the reaction with deionized water.

2.2.14. FACS analysis of immune cells after various treatments

At the end of treatment in the B16-OVA tumor model, peripheral blood, spleen, and lymph nodes from different treatment groups were extracted for immune cell analysis. The staining procedure was carried out according to the previous steps. Peripheral blood was collected from mice and anticoagulated using sodium heparin solution. The spleen was gently ground, and all cells were collected by filtering through a 300-mesh nylon filter to achieve a single-cell suspension. The peripheral blood and spleen samples were suspended in red blood lysis solution for red blood cell lysis, and a single-cell suspension in FACS buffer was obtained. The lymph nodes were gently ground, all cells were collected, and a single-cell suspension was obtained by filtration with a 300-mesh nylon filter. The samples obtained were stained with different fluorochrome-conjugated antibodies according to the manufacturer's instructions.

2.2.15. Statistical analysis

For all experiments, at least three flat sampling operations were performed and expressed as the mean ± standard deviation (s.d.). All statistical significance between the two groups was analyzed using Student's t-test.

3. Results and discussion

3.1. Preparation and characterization of mannan-decorated STING-activating vaccine carrier

The design of the STING-activating inner core, PLA-PEI-4BImi (we name it as PPB), was based on our previous study in identifying that azole molecule-conjugated branched polyethylenimine (PEI-M) exhibits STING-stimulating activity [23]. Briefly, hydrophobic PLA was first conjugated to branch PEI with a mole ratio of 1:1 to increase the stability of the formed nanoparticles, and the successful conjugation of PLA was evidenced by the appearance of the B and C peaks in ^{1}H NMR. 4BImi, the best-performing azole from the PEI-M library, was then conjugated to PLA-PEI through an amidation reaction at a mole ratio of 20/1, and the degree of conjugation was calculated by ^{1}H NMR with the hydrogen atom peak from the azole at 8.94 and 7.39 ppm (Fig. 1a-b).

Herein, the model antigen OVA was applied for preparation of the nanovaccines. For the purpose of obtaining suitable antigen loading, nanoparticles with weight ratios of PPB to antigen protein from 1:1 to 4:1 were prepared for DLS measurement, and the weight ratio of 3:1 was the optimal assembly condition after testing with different ratios (Fig. S1). As shown in Fig. 1c, OVA loading slightly increased the hydrodynamic diameter of the PPB core while decreasing the surface zeta potentials. Furthermore, oxidized mannan was decorated onto PPB/OVA through a Schiff's base reaction between the aldehyde on the mannan

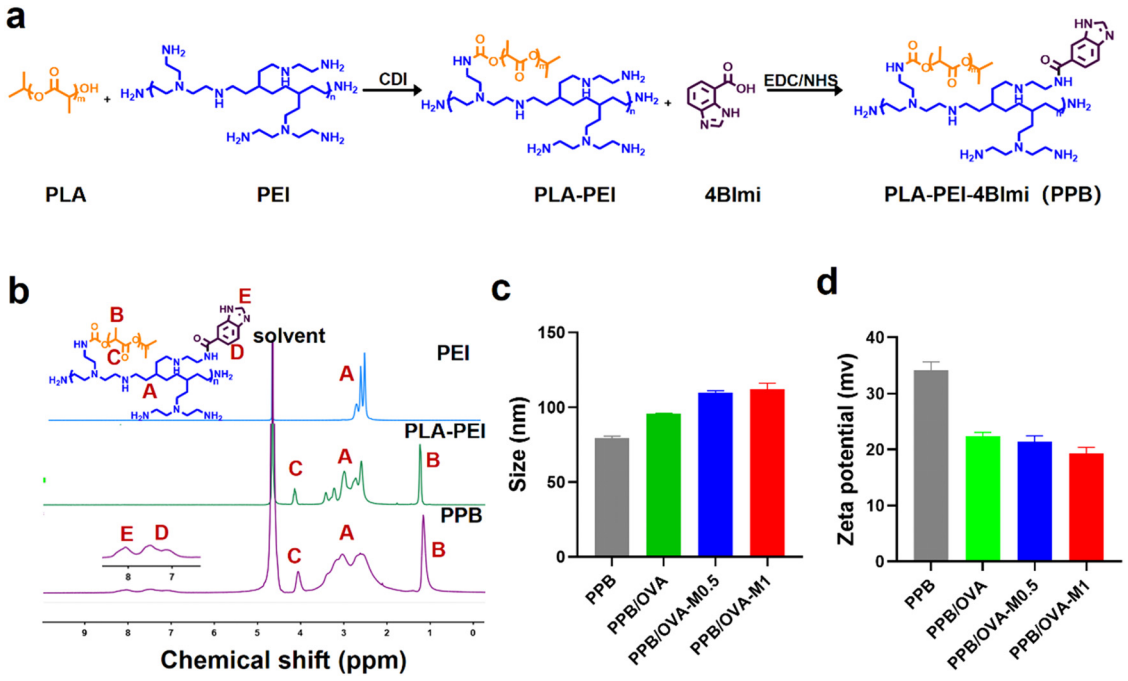

Fig. 1. Preparation and characterization of nanoformulations. (a) Synthesis routes of PLA-PEI-4BImi (PPB). (b) ^{1}H NMR spectrum of PEI, PLA-PEI and PPB. (c-d) Diameter and zeta potentials of various vaccine formulations. (n = 3).

and the amino groups on the PEI, and the assembly was carried out under conditions with 1:0.5 and 1:1 wt ratios of PPB cores and mannan (we name it PPB/OVA-M0.5 and PPB/OVA-M1, respectively). Mannan decoration further increased the diameter of the nanoparticles while decreasing the zeta potential (Fig. 1b-c). The transmission electron microscopy (TEM) results of PPB/OVA, PPB/OVA-M0.5, and PPB/OVA-M1 were compatible with the DLS results (Fig. S2). The assembly of PPB/OVA-M0.5 and PPB/OVA-M1 was stable for 48 h, while PEI-4BImi/OVA-M0.5 and PEI-4BImi/OVA-M1 (we name it PB/OVA-M0.5 and PB/OVA-M1, respectively) were disassembled within 12 h. The particle stability results demonstrated the necessity of hydrophobic PLA for stable particle assembly (Fig. S3).

3.2. In vitro evaluation of DC maturation and antigen cross-presentation

Type I interferons (IFN-Is), which are produced as a result of signaling via the STING pathway, play a powerful anti-tumor role by regulating tumor cell proliferation, inhibiting tumor metastasis and angiogenesis, and activating anti-tumor immune response [24]. The innate stimulation effect of the PPB was first verified through the measurement of IFN-β secretion. As shown in Fig. 2a, PPB induced intense IFN-β secretion from DC2.4 cells at concentrations over 100 pg/mL. Complexation with OVA does not affect the innate stimulating activity of PPB, and mannan-decoration slightly decreased IFN-β secretion.

To confirm whether this innate stimulating activity is caused by the STING pathway, we further evaluated STING pathway activation inside the cells after various treatments. STING protein is transferred from the endoplasmic reticulum to the Golgi apparatus during the process of agonist-stimulated STING activation and then recruits and phosphorylates TANK-binding kinase 1 (TBK1). Subsequently, STING and interferon regulatory factor 3 (IRF3) are phosphorylated by activated TBK1, and phosphorylated IRF3 is transferred to the nucleus to initiate transcription of the IFN-I gene (Fig. 2b). Thus, the level of STING pathway activation can be assessed by measuring the phosphorylation of TBK1, STING and IRF-3 in the cell as a marker. As shown by phosphorylation flow cytometry in Fig. 2c, the ^{P}STING, ^{P}TBK1, and ^{P}IRF-3 signals of the experimental group were all greatly increased compared with those of the control group, and the phosphorylation levels of the STING pathway in PPB/OVA and PPB-OVA-M were comparable, which may be due to the similar levels of cellular endocytosis (Fig. S4). To further demonstrate the activation of the STING pathway, Western blot was performed with PPB/OVA, PPB/OVA-M0.5, PPB/OVA-M1 and PEI-loaded commercial STING pathway agonist cGAMP as a positive control. As shown in Fig. S5, PPB/OVA, PPB/OVA-M0.5 and PPB/OVA-M1 had a similar degree of phosphorylation of STING pathway-associated proteins compared with the positive control; in the presence of brefeldin A (BFA), which blocks protein trafficking between the ER and Golgi [26], both cGAMP and different nanoformulations failed to trigger phosphorylated production. While activated by agonists, STING proteins accumulate on the ER and assemble into oligomeric structures, known as protein clusters. After cellular uptake, PPB nanovaccines can escape from the lysosome to interact with STING proteins in the endoplasmic reticulum. STING clustering was also observed after treatment with various vaccine formulations (Fig. S6). All the results show that the inner core PPB could stimulate the activation of the STING pathway, and this ability was still maintained after mannan-decoration.

The cellular uptake capacity was further investigated with flow cytometry. Compared to OVA, PPB/OVA, PPB/OVA-M0.5, and PPB/OVA-M1 were able to significantly increase cellular uptake capacity (Fig. 2d). To evaluate the effect on the maturation of DCs, bone marrow-derived dendritic cells (BMDCs) were seeded in plates and co-incubated with the different vaccine formulations: 1) PBS, 2) OVA, 3) PBB/OVA, 4) PBB/OVA-M0.5, and 5) PPB/OVA-M1. As shown in Fig. 2e, PPB/OVA, PPB/OVA-M0.5, and PPB/OVA-M1 could significantly enhance the ability of DCs maturation, as indicated by the improved expression of MHC class II and CD80 on BMDCs (Fig. S7). In the meantime, mannan could interact with the TLR4 receptor of DCs [25], which could synergize with the STING pathway (Fig. S8).

For direct assessment of the level of antigen cross-presentation, the surface presentation of the OVA257-264 (SIINFEKL) peptide complex loaded with MHC-I in BMDCs can be measured by flow cytometry. As shown in Fig. 2f, PPB/OVA greatly increased OVA antigen cross-presentation, which was 14-fold higher than that of free OVA (Fig. S9). In addition, the mannan-decoration could further promote the cross-presentation of OVA protein. Taken together, we preliminarily proved that the mannan-decorated STING-activating vaccine carrier we designed could solve the intracellular coordination obstacle of activating APCs and cross-presenting antigens in vitro.

3.3. Lymph node draining and immune activation in vivo

Lymph nodes are essential organs in vaccination anti-tumor activity. Antigens are processed by APCs in the lymph nodes and then delivered to T cells and B cells, leading to cellular and humoral immunity, respectively. An essential component of cancer vaccination treatment is the efficient transport of antigens to lymph nodes. Due to the negative charge of the interstitium, the capacity of positively charged nanocarriers to reflux into the draining lymph nodes is significantly diminished [12]. Numerous investigations have shown that negatively charged modifications could improve nanoparticle lymph node reflux [27]. It is also a successful strategy to promote lymph node draining to modify nanoparticles with active targeting molecules such as mannose or mannan [28]. To evaluate the lymph node accumulation capability of the different prepared vaccine formulations, the inguinal lymph nodes on both sides were excised at 24 h after subcutaneous injection at the base of the tail of C57BL/6 mice. According to the fluorescence results of the dissected lymph nodes (Fig. 3a-b), the mean fluorescence intensity of PPB/OVA-treated lymph nodes was improved 2.7-fold compared with free OVA, certifying that PPB loading could increase lymph node reflux capacity to some extent, but the reflux effect is still unsatisfactory. The mannan-decoration further increased lymph node accumulation, and the fluorescence intensity of PPB/OVA-M1 was 4.3-fold stronger than that of free OVA. Flow cytometric analysis of inguinal lymph nodes was performed to study in detail the distribution of antigens among different subsets of DCs. Similar to the ex vivo fluorescence data in the lymph node, the percentage of OVA-positive cells was significantly increased in the mannan decoration groups (Fig. 3c). Mannan-decoration significantly improved the DC targeting ability of nanovaccines in the lymph nodes. In particular, PPB/OVA-M1 greatly enhanced the OVA-positive $CD8^+$ DC population, which could greatly improve the level of antigen cross-presentation because $CD8^+$ DCs are professional antigen cross-presenting cells in the lymph nodes [29]. The assessment of the OVA-positive pDCs population showed that more nanovaccines also accumulated in the pDCs, which is highly important for the secretion of interferon and induction of T-cell differentiation (Fig. S12). According to the above results, the lymph node transport capacity of PPB/OVA-M1 was gradually improved compared with that of PPB/OVA, and the same was true for $CD8^+$ and pDC cells. All these results showed that mannan-decoration has unique advantages for lymph node reflux and for improving vaccine distribution of $CD8^+$ DCs and pDC subsets.

The above results showed that PPB/OVA-M1 seems to be the top-performing vaccine formulation. Therefore, PPB/OVA-M1 was used for the following studies. For in vivo DC activation and antigen cross-presentation, the inguinal lymph nodes were excised for flow cytometry analysis 48 h after subcutaneous inoculation. According to the results of flow cytometry, PPB/OVA-M1 could significantly improve the expression of MHC II, CD80, and CD86 in DCs in lymph nodes compared with PPB/OVA, as well as the obvious cross-presentation ability for OVA257-264 peptide (SIINFEKL) (Figs. 3d-e and S13). All these results proved that PPB/OVA-M1 has a better spatially synergistic ability to activate antigen-specific immunity and could effectively accumulate in lymph nodes, activate the maturation of DCs and the cross-

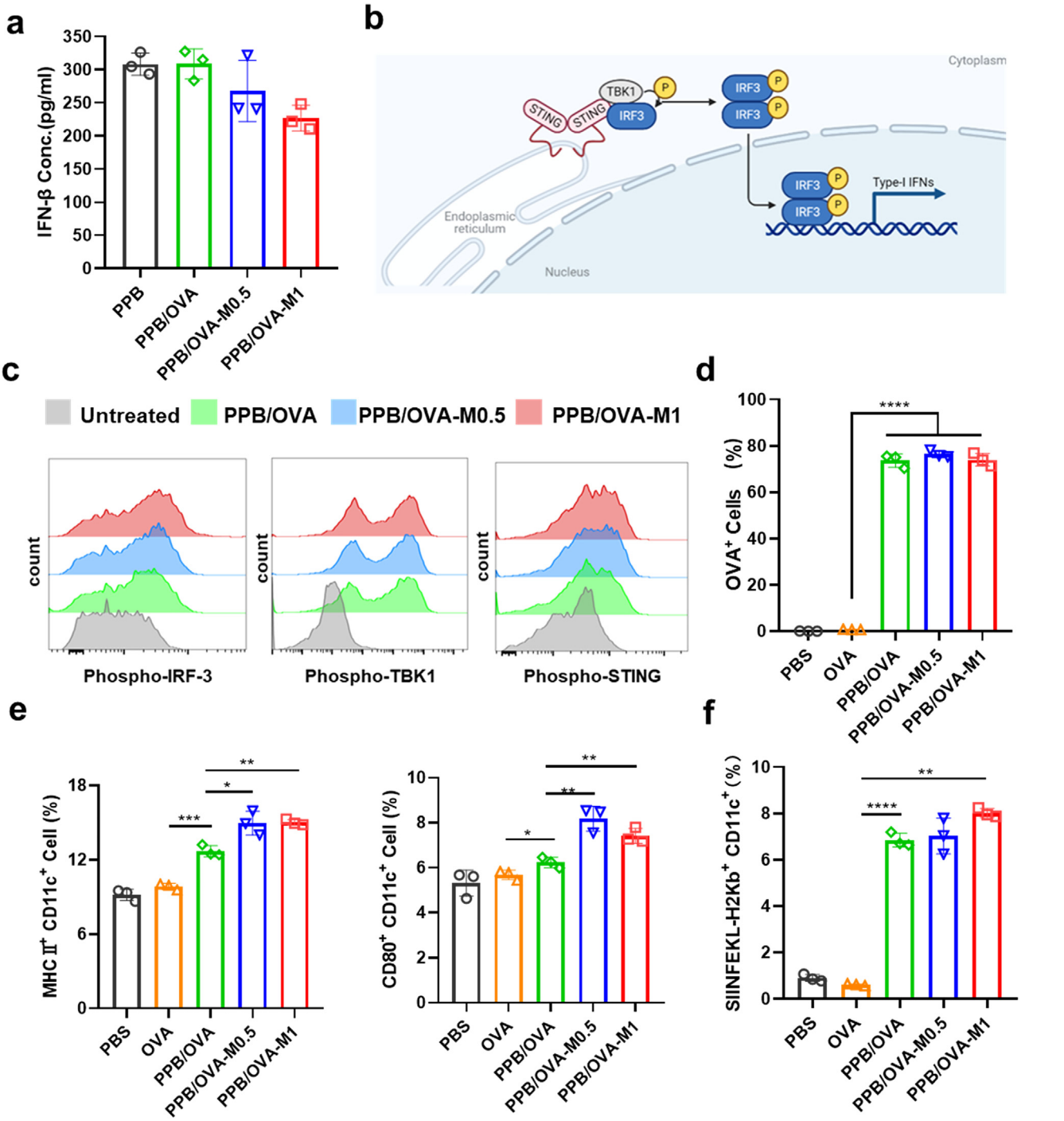

Fig. 2. Stimulation on DCs maturation and STING pathway verification. (a) The concentration of IFN-β in the medium of DC2.4 cells after incubation. (b) Schematic representation of ligand-mediated activation of STING and its downstream signaling pathways. (c) Flow cytometry analysis of phosphorylated proteins associated with STING pathway activation in BMDCs. (d) Flow cytometry analysis of DC2.4 cells after incubation with different vaccine formulations for 4 h. (e) BMDC activation effect in different vaccine treatment groups. (f) Antigen cross-presentation results of BMDCs in various treatment groups. Results are presented as means ± SD; $^{*}p < 0.05$, $^{**}p < 0.01$, $^{***}p < 0.001$, $^{****}p < 0.0001$; ns, no significance. Data were presented as means ± SD ($n = 3$).

presentation of antigens in vivo, which highlights the possibility of using it for evaluation in subsequent in vivo therapeutic experiments. To confirm that the innate stimulating activity is caused by the STING pathway in vivo, we further evaluated STING pathway activation in vivo after various treatments. Both the phosphorylation flow cytometry and western blot results demonstrated that PPB/OVA could activate STING pathway phosphorylation in vivo, and the degree of phosphorylation with PPB/OVA-M1 was further increased by mannan modification due to the better lymph node reflux capacity of PPB/OVA-M1 (Fig. 3f-g).

3.4. Therapeutic efficacy of PPB/OVA-M1 in a B16-OVA tumor model and immunological analysis

The therapeutic effect of PPB/OVA-M1 as a vaccine carrier was evaluated in the B16-OVA melanoma model. The tumor model was estab-

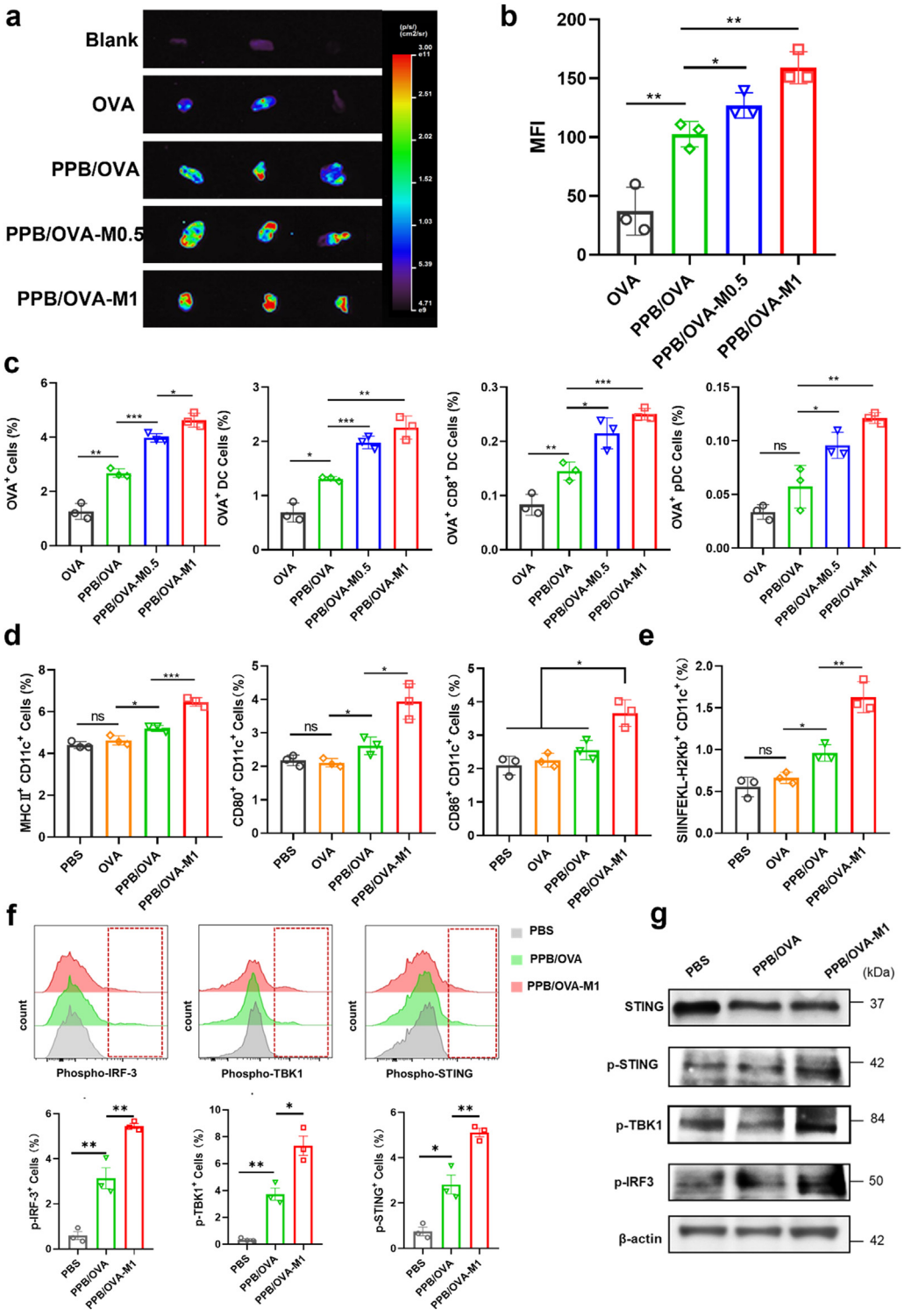

Fig. 3. Lymph node draining and DCs activation in vivo. (a-b) In vitro fluorescence images of lymph nodes in different treatment groups and statistical fluorescence intensity. (c) OVA-positive cell populations of different treatment groups. (d-e) FACS analysis of DC surface markers (CD80, CD86, MHCII) and antigen cross-presentation (SIINFEKL-H2Kb) in inguinal draining LNs at 48 h after subcutaneous injection of different vaccine formulations ($n = 3$). (f) Flow cytometry analysis of phosphorylated proteins associated with STING pathway activation in vivo. (g) Western blot images of phosphorylated proteins associated with STING pathway activation in vivo. Results are presented as means ± SD; $^{*}p < 0.05$, $^{**}p < 0.01$, $^{***}p < 0.001$; ns, no significance. Data were presented as means ± SD ($n = 3$).

lished by subcutaneous injection of 2.5×10^5 B16-OVA cells into the right abdomen of female C57BL/6 mice. After tumor cell inoculation, different vaccine formulations were injected subcutaneously into the tail base of mice at 5, 10, and 15 days. As shown in Fig. 4b-c, PPB/OVA and PPB/OVA-M1 both showed better inhibition of B16-OVA tumor growth than Alum/OVA, while PPB/OVA-M1 showed the strongest therapeutic effect, with a tumor suppression rate (TSR%) of 93% on Day 21. After various treatments on Day 21, immune cells in the peripheral blood and spleen and DCs in lymph nodes were analyzed. The populations of IFN-γ^+ CD4$^+$ T cells and IFN-γ^+ CD8$^+$ T cells were greatly enhanced

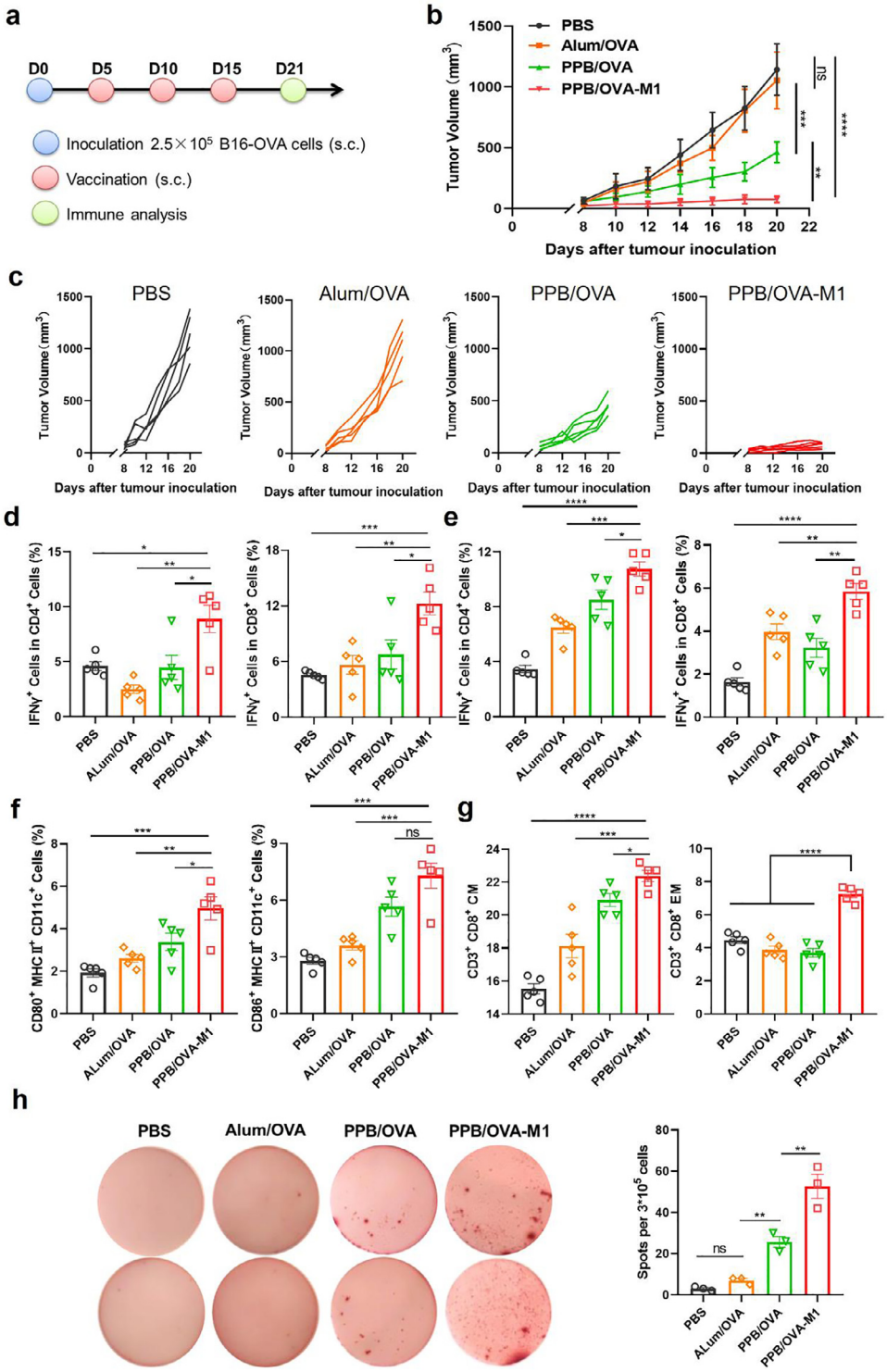

Fig. 4. Antitumor effects and immune analysis of vaccine therapy in B16-OVA tumor model. (a) Schematic illustration of tumor inoculation and treatment schedule. (b) B16-OVA tumor growth curves of different treatment groups (n = 5). (c) Individual tumor growth curves of mice in different treatment groups. (d) Activated $CD4^+$ and $CD8^+$ T cell populations in the peripheral blood of different treatment groups. (e) Activated $CD4^+$ and $CD8^+$ T cell populations in the spleen of different treatment groups. (f) The activation of DCs in lymph nodes. (g) Memory effect analysis in spleens. (h) ELISPOT results of different treatment groups. Results are presented as means ± SD; $^*p < 0.05$, $^{**}p < 0.01$, $^{***}p < 0.001$, $^{****}p < 0.0001$; ns, no significance. Data were presented as means ± SD (n = 3).

in both the blood and spleen (Figs. 4d-e and S14–15). The DCs in the lymph node also had a certain increase, especially in the PPB/OVA-M1 treatment group (Figs. 4f and S16). The subpopulations of memory T cells in the spleen were further analyzed. A significant increase in $CD8^+$ effector memory (EM) T cells and central memory (CM) T cells was observed after PPB/OVA-M1 treatment (Figs. 4g and S17). To further prove that PPB/OVA-M1 can elicit antigen-specific immune responses, ELISPOT analysis of splenocytes was performed (Fig. 4h). In the spots observed, the number of PPB/OVA-M1 was significantly increased compared to other groups, further confirming that PPB/OVA-M1 was supe-

rior in eliciting a robust response of antigen-specific immunity. All the above results firmly indicate that PPB/OVA-M1 can induce a strong response of antigen-specific T cells and effectively inhibit tumor growth.

4. Conclusion

In this study, we developed a mannan-decorated STING-activating vaccine carrier for spatial coordinative stimulation of antigen-specific immune responses. The mannan decoration could greatly increase antigen accumulation in the lymph nodes, particularly enhancing the distribution in $CD8^+$ DCs. In the meantime, the STING-activating core could reconcile the problem of conflicting antigen and adjuvant active site locations after lysosome escape and solve the spatial coordination obstacle of APC activating and cross-presenting antigen to $CD8^+$ cytotoxic T cells. In the B16-OVA tumor model, single usage of PPB/OVA-M1 could achieve a 93% tumor suppression rate.

The efficient accumulation of antigens in lymph nodes and the spatial coordination of innate stimulation of APCs and antigen cross-presentation are the current struggle of cancer vaccine design. Most of the current studies are focused on one single step in antigen delivery to the lymph node, but systematic coordination of all transport steps, including antigen delivery to the lymph node as well as inside APCs, is the key to achieving robust anti-tumor immunity. Our results demonstrate the importance of systematically spatially coordinated stimulation of antigen-specific immune responses. Systematic solutions to the spatial transmission problem of antigens can greatly improve cancer vaccine efficacy.

Declaration of competing interest

The authors declare that they have no conflicts of interest in this work.

Acknowledgments

This work was supported by grants from the National Natural Science Foundation of China (22222509, 51973215, 52025035, 52103194, 22105199), the Ministry of Science and Technology of China (2022YFE0110200), Bureau of International Cooperation Chinese Academy of Sciences (121522KYSB20200029), Jilin Province Science and Technology Development Plan (YDZJ202101ZYTS131, 20220402037GH), Jilin Provincial International Cooperation Key Laboratory of Biomedical Polymers (20210504001GH), Changchun Science and Technology Development Plan (21ZY09), and the Youth Innovation Promotion Association of Chinese Academy of Sciences (2020232).

Supplementary materials

Supplementary material associated with this article can be found, in the online version, at doi:10.1016/j.fmre.2023.03.018.

References

[1] S.A. Rosenberg, J.C. Yang, N.P. Restifo, Cancer immunotherapy: Moving beyond current vaccines, Nat. Med. 10 (9) (2004) 909–915.
[2] Z. Liu, Y. Ren, S. Weng, et al., A new trend in cancer treatment: The combination of epigenetics and immunotherapy, Front. Immunol. 13 (2022) 809761-61.
[3] S.C. Wei, C.R. Duffy, J.P. Allison, Fundamental mechanisms of immune checkpoint blockade therapy, Cancer Discov. 8 (9) (2018) 1069–1086.
[4] H.J. Jackson, S. Rafiq, R.J. Brentjens, Driving CAR T-cells forward, Nat. Rev. Clin. Oncol. 13 (6) (2016) 370–383.
[5] Q. Song, C.D. Zhang, X.H. Wu, Therapeutic cancer vaccines: From initial findings to prospects, Immunol. Lett. 196 (2018) 11–21.
[6] Y. Zhang, S. Ma, X. Liu, et al., Supramolecular assembled programmable nanomedicine as in situ cancer vaccine for cancer immunotherapy, Adv. Mater. 33 (7) (2021) e2007293.
[7] S. Ma, Y.D. Xu, W.T. Song, Functional bionanomaterials for cell surface engineering in cancer immunotherapy, Apl. Bioeng. 5 (2) (2021).
[8] Q.L. Zhang, S. Hong, X. Dong, et al., Bioinspired nano-vaccine construction by antigen pre-degradation for boosting cancer personalized immunotherapy, Biomaterials 287 (2022) 121628.
[9] L. Qin, J. Cao, K. Shao, et al., A tumor-to-lymph procedure navigated versatile gel system for combinatorial therapy against tumor recurrence and metastasis, Sci. Adv. 6 (36) (2020) eabb3116.
[10] S. Dong, S. Ma, Z.L. Liu, et al., Functional amphiphilic poly(2-oxazoline) block copolymers as drug carriers: The relationship between structure and drug loading capacity, Chin. J. Polym. Sci. 39 (7) (2021) 865–873.
[11] J.Y. Zhao, W.T. Song, Z.H. Tang, et al., Macromolecular effects in medicinal chemistry, Acta Chim. Sinica 80 (4) (2022) 563–569.
[12] M. Zhu, Immunological perspectives on spatial and temporal vaccine delivery, Adv. Drug. Deliv. Rev. 178 (2021) 113966.
[13] A. Schudel, D.M. Francis, S.N. Thomas, Material design for lymph node drug delivery, Nat. Rev. Mater. 4 (6) (2019) 415–428.
[14] Y. Chen, S. De Koker, B.G. De Geest, Engineering strategies for lymph node targeted immune activation, Acc. Chem. Res. 53 (10) (2020) 2055–2067.
[15] Y. Xu, S. Ma, J. Zhao, et al., Mannan-decorated pathogen-like polymeric nanoparticles as nanovaccine carriers for eliciting superior anticancer immunity, Biomaterials 284 (2022) 121489.
[16] J.A. Hubbell, S.N. Thomas, M.A. Swartz, Materials engineering for immunomodulation, Nature 462 (7272) (2009) 449–460.
[17] D.J. Irvine, A. Aung, M. Silva, Controlling timing and location in vaccines, Adv. Drug. Deliv. Rev. 158 (2020) 91–115.
[18] M. Luo, H. Wang, Z. Wang, et al., A STING-activating nanovaccine for cancer immunotherapy, Nat. Nanotechnol. 12 (7) (2017) 648–654.
[19] L. Miao, L. Li, Y. Huang, et al., Delivery of mRNA vaccines with heterocyclic lipids increases anti-tumor efficacy by STING-mediated immune cell activation, Nat. Biotechnol. 37 (10) (2019) 1174–1185.
[20] Z.Y. Fan, S.R. Jan, J.C. Hickey, et al., Multifunctional dendronized polypeptides for controlled adjuvanticity, Biomacromolecules 22 (12) (2021) 5074–5086.
[21] C.K. Tang, J. Lodding, G. Minigo, et al., Mannan-mediated gene delivery for cancer immunotherapy, Immunology 120 (3) (2007) 325–335.
[22] X. Sun, S. Chen, J. Han, et al., Mannosylated biodegradable polyethyleneimine for targeted DNA delivery to dendritic cells, Int. J. Nanomed. 7 (2012) 2929–2942.
[23] J.Y. Zhao, Y.D. Xu, S. Ma, et al., A minimalist binary vaccine carrier for personalized postoperative cancer vaccine therapy, Adv. Mater. 34 (10) (2022) e2109254.
[24] A. Thim-Uam, T. Prabakaran, M. Tansakul, et al., STING mediates lupus via the activation of conventional dendritic cell maturation and plasmacytoid dendritic cell differentiation, Iscience 23 (9) (2020) 101530.
[25] L. Romani, Immunity to fungal infections, Nat. Rev. Immunol. 4 (1) (2004) 11–24.
[26] S. Li, M. Luo, Z. Wang, et al., Prolonged activation of innate immune pathways by a polyvalent STING agonist, Nat. Biomed. Eng. 5 (2021) 455–466.
[27] B.Y. Chua, M.R. Olson, S. Bedoui, et al., The use of a TLR2 agonist-based adjuvant for enhancing effector and memory CD8 T-cell responses, Immunol. Cell Biol. 92 (4) (2014) 377–383.
[28] H. Tada, E. Nemoto, H. Shimauchi, et al., Saccharomyces cerevisiae- and Candida albicans-derived mannan induced production of tumor necrosis factor alpha by human monocytes in a CD14-and Toll-like receptor 4-dependent manner, Microbiol. Immunol. 46 (7) (2002) 503–512.
[29] P. Schnorrer, G. Behrens, N.S. Wilson, et al., The dominant role of $CD8^+$ dendritic cells in cross-presentation is not dictated by antigen capture, in: Proceedings of the National Academy of Sciences, 2006.

Author profile

Liping Liu is a Ph.D. student of Changchun Institute of Applied Chemistry, Chinese Academy of Sciences. Her research mainly focuses on the nanomaterial-based vaccine used in tumor immunotherapy.

Wantong Song (BRID: 03280.00.73711) is a full professor at Changchun Institute of Applied Chemistry (CIAC), Chinese Academy of Sciences (CAS). He obtained his B.S. degree from Nanjing University in 2008, and Ph.D. degree from the University of Chinese Academy of Sciences in 2013, and started his research career in CIAC since then. He had his postdoctoral training by working with Prof. Leaf Huang at the University of North Carolina at Chapel Hill from 2016 to 2018. Dr. Song's research focuses on developing innovative polymeric carriers for drug, gene and vaccine delivery. He has published more than 70 papers in *Nat. Nanotechnol., Nat. Commun., Adv. Mater.*, et al., and applied for more than 20 patents.